Polyhedron 169 (2019) 135–143

Contents lists available at ScienceDirect

Polyhedron

journal homepage: www.elsevier.com/locate/poly

Extending the family of heptanuclear heterometallic Cu_5Ln_2 (Ln = Gd, Tb, Dy) complexes: Synthesis, crystal structures, magnetic and magnetocaloric studies

Despina Dermitzaki [a], Vassilis Psycharis [a], Yiannis Sanakis [a], Th. C. Stamatatos [b], Michael Pissas [a], Catherine P. Raptopoulou [a,*]

[a] Institute of Nanoscience and Nanotechnology, NCSR "Demokritos", 15310 Aghia Paraskevi, Athens, Greece
[b] Department of Chemistry, University of Patras, 26504 Patras, Greece

ARTICLE INFO

Article history:
Received 9 April 2019
Accepted 3 May 2019
Available online 13 May 2019

Keywords:
Copper(II)–Lanthanide(III) complexes
Crystal structures
Magnetic measurements
Magnetocaloric effect
Single-molecule magnet

ABSTRACT

The reaction of $Ln(NO_3)_3{\cdot}6H_2O$ (Ln = Gd, Tb, Dy) and $Cu(O_2CMe)_2{\cdot}H_2O$ with the polydentate Schiff base ligands OH-$C_{10}H_6$-CH=NC(R)$(CH_2OH)_2$ (R = CH_3, H_3L1; R = C_2H_5, H_3L2) in Me_2CO afforded the heptanuclear heterometallic complexes $[Cu_5Ln_2(O_2CMe)_2(NO_3)_4(L1)_2(HL1)_2(Me_2CO)_2]$ (Ln = Gd (**1**), Tb (**2**), Dy (**3**)) and $[Cu_5Ln_2(O_2CMe)_2(NO_3)_4(L2)_2(HL2)_2]$ (Ln = Gd (**4**), Tb (**5**), Dy (**6**)). Crystallographic studies revealed that complexes **1**–**3** and **4**–**6** consist of a central core $\{Cu^{II}_5Ln^{III}_2(\mu_3\text{-OR})_6(\mu_3\text{-}O_2CMe)_2\}^{8+}$ described as two distorted cubane subunits, $\{Cu^{II}_3Ln^{III}(\mu_3\text{-OR})_3(\mu_3\text{-}O_2CMe)\}^{5+}$, with a Cu^{II} ion in the common apex. Peripheral and bridging ligation is provided by two triply and two doubly deprotonated Schiff base ligands, two μ_3-acetates and four chelating nitrates. Magnetic susceptibility measurements revealed the presence of dominant ferromagnetic interactions in all complexes. The magnetocaloric effect of **1** was examined via isothermal magnetization measurements under various applied fields and the maximum entropy change was 16.3 J kg^{-1} K^{-1} at 2 K for ΔH = 5 T. Ac susceptibility measurements of **2**, **3** and **6** revealed slow magnetic relaxation processes suggesting the presence of single-molecule magnet behavior.

1. Introduction

Molecular magnetic materials based on homo- and/or heterometallic coordination complexes are prepared by using serendipitous or rational designed methods according to the so-called 'bottom-up' approach. These discrete molecular coordination compounds offer various advantages such as particle monodispersity, crystallinity, solubility and a shell of organic ligands around the metal ions that can be modified in order to afford molecules with desired functionality [1]. These materials often exhibit noteworthy physical properties and have been extensively studied over the past decades, therefore they have been proposed as candidates for potential applications in high-density information storage devices, quantum computing, spintronics and magnetic refrigeration [2].

The molecular magnetic materials have been proposed as promising candidates for magnetic refrigeration as an alternative to the increasingly rare and expensive helium-3 which is currently used for low-temperature refrigeration. The magnetic refrigeration is based on the magnetocaloric effect (MCE), i.e. the isothermal change of magnetic entropy (ΔS_m) and adiabatic change of temperature (ΔT_{ad}) that follow a change of the applied magnetic field (ΔH), and is based on cycles of adiabatic magnetization, isomagnetic enthalpic transfer, adiabatic demagnetization and isomagnetic entropic transfer. The ideal material for magnetic refrigeration applications should exhibit large MCE in order to show great potential temperature change, and this can be achieved by combining large spin ground state, negligible magnetic anisotropy, high spin degeneracy due to low-lying excited states, large metal-to-ligand ratio and low molecular weight. Most of the complexes examined as magnetic refrigerants, contain the isotropic Gd^{III} (S = 7/2) ion [3–5], although other approaches have been also examined [6]. The development of magnetic refrigerants based on coordination clusters offers the advantage of energy-efficient and environmentally friendly materials which do not require the use of hazardous chemicals or greenhouse gases.

For information storage and quantum computing applications, the molecular magnetic materials should exhibit large spin ground state and large magnetic anisotropy in order to achieve magnetization reversal. This has been addressed in hundreds of homo- and heterometallic complexes of transition metals and lanthanides.

* Corresponding author: Fax: +30 210 6519430.
E-mail address: c.raptopoulou@inn.demokritos.gr (C.P. Raptopoulou).

https://doi.org/10.1016/j.poly.2019.05.004
0277-5387/

The combination of 3d and 4f metal ions has been proved successful in order to achieve high-spin ground states, originated from the 3d metal ions, and large single-ion anisotropy, gained from the lanthanides.

We have previously reported our preliminary results concerning the synthesis and magnetic properties of the heterometallic heptanuclear complexes $[Cu_5Ln_2(O_2CMe)_2(NO_3)_4(L2)_2(HL2)_2]$ (Ln = Gd (**4**), Tb (**5**); H_3L2 = OH-$C_{10}H_6$-CH=NC(R)$(CH_2OH)_2$, R = C_2H_5). Both complexes are isostructural, however their magnetic behavior is governed by the nature of the lanthanide ion. Magnetocaloric studies for complex **4** showed an entropy change $-\Delta S_m$ = 15.7 J kg^{-1} K^{-1} at 2 K for ΔH = 5 T, whereas complex **5** exhibits single-molecule magnet behavior as evidenced by the presence of out-of-phase tails of signals at 2 K in the ac-susceptibility measurements under zero applied external magnetic field [7]. Our synthetic approach is based on the hard soft acid base (HSAB) principle and our ligands of choice are Schiff bases derived from the condensation of 2-hydroxy-1-naphthaldehyde and the amino-alcohols, 2-amino-2-methyl-1,3-propanediol (H_3L1) and 2-amino-2-ethyl-1,3-propanediol (H_3L2). These ligands contain a coordination pocket of nitrogen/oxygen donor atoms which favor binding to the 3d metal ion and pendant hydroxyl groups which favor coordination to the lanthanide ion. A handful of Cu^{II}–Ln^{III} Schiff base complexes have been extensively studied, for example dinuclear [8], trinuclear [9–12], tetranuclear [13–16] and higher nuclearity clusters [17–20]. The magnetic behavior of the Cu^{II}–Ln^{III} complexes is governed by the nature of the lanthanide. The magnetic anisotropy introduced by the Tb^{III}, and Dy^{III} ions makes them excellent candidates for molecular nanomagnets, whereas the isotropic character of the Gd^{III} ion is suitable for magnetic refrigerants. We present herein the synthesis, magnetic and magnetocaloric (for **1**) study of the heptanuclear clusters $[Cu_5Ln_2(O_2CMe)_2(NO_3)_4(L1)_2(HL1)_2(Me_2CO)_2]$ (Ln = Gd (**1**), Tb (**2**), Dy (**3**)) and $[Cu_5Ln_2(O_2CMe)_2(NO_3)_4(L2)_2(HL2)_2]$ (Ln = Dy (**6**)) and compare these results with those previously reported for complexes **4** and **5**.

2. Experimental

2.1. General and spectroscopic measurements

All manipulations were performed under aerobic conditions using materials as received (Aldrich Co). All chemicals and solvents were of reagent grade. The ligands OH-$C_{10}H_6$-CH=NC(R)$(CH_2OH)_2$, (R = CH_3, H_3L1; R = C_2H_5, H_3L2) were synthesized as reported previously [21]. Elemental analysis for carbon, hydrogen, and nitrogen was performed on a Perkin Elmer 2400/*II* automatic analyzer. Infrared spectra were recorded as KBr pellets in the range 4000–400 cm^{-1} on a Bruker Equinox 55/S FT-IR spectrophotometer. Variable-temperature and field magnetic measurements were carried out on polycrystalline samples using Quantum Design PPMS 9 T and SQUID magnetometer Quantum Design MPMS 5.5. Diamagnetic corrections were estimated from Pascal's constants.

2.2. Compound preparations

2.2.1. $[Cu_5Gd_2(O_2CMe)_2(NO_3)_4(L1)_2(HL1)_2(Me_2CO)_2]\cdot 6Me_2CO$ (**1**·6Me_2CO)

Solid $Gd(NO_3)_3\cdot 6H_2O$ (0.10 mmol, 0.0451 g) was added under stirring to a yellow solution of H_3L1 (0.10 mmol, 0.0259 g) in Me_2CO (20 mL). After 10 min of stirring, solid $Cu(O_2CMe)_2\cdot H_2O$ (0.10 mmol, 0.0200 g) was added and the solution became dark green. The stirring continued for 30 min and the final reaction solution was kept in closed vials. Crystals of **1** were formed after three days. Yield: 0.016 g, ~35% based on Cu^{II}. $C_{76}H_{88}N_8O_{32}Cu_5Gd_2$, **1**·2$Me_2CO$ (f.w. = 2257.80) requires C, 40.43; H, 3.93; N, 4.96. Found: C, 40.34; H, 3.90; N, 4.93%. FT-IR (KBr pellets, selected peaks, cm^{-1}): ν(OH) 3418(br), ν(C=N) 1605(vs), ν_{as}(COO) 1510(s), ν_s(COO) 1340(s), ν(C–O) 1360(s), ν(C=O) 1700(m), $\nu(NO_3)_{coordinated}$ 1359(m)/1245(m), $\nu(NO_3)_{ionic}$ 1380(vs).

2.2.2. $[Cu_5Tb_2(O_2CMe)_2(NO_3)_4(L1)_2(HL1)_2(Me_2CO)_2]$ (**2**)

Solid $Tb(NO_3)_3\cdot 6H_2O$ (0.10 mmol, 0.0453 g) was added under stirring to a yellow solution of H_3L1 (0.10 mmol, 0.0259 g) in Me_2CO (25 mL). After 10 min of stirring, solid $Cu(O_2CMe)_2\cdot H_2O$ (0.10 mmol, 0.0200 g) was added and the solution became dark green. The stirring continued for 30 min and the final reaction solution was layered with mixture Et_2O/*n*-hexane (1:1 v/v). Crystals of **2** were formed after five days. The identity of the crystals was confirmed by unit cell determination (a = 14.06, b = 14.47, c = 15.09 Å, α = 65.29, β = 66.79, γ = 67.96°, V = 2480 $Å^3$, Table 1). Unfortunately, the crystals of **2** were poorly diffracted and were not suitable for complete crystal structure determination. Yield: 0.0230 g, ~50% based on Cu^{II}. $C_{70}H_{76}N_8O_{30}Cu_5Tb_2$, **2** (f.w. = 2144.98) requires C, 39.20; H, 3.57; N, 5.22. Found: C, 39.12; H, 3.54; N, 5.19%. FT-IR (KBr pellets, selected peaks, cm^{-1}): ν(OH)

Table 1
Crystallographic data for **1**·6Me_2CO, **3**·3.2Me_2CO and **6**·4Me_2CO.

	1·6Me_2CO	**3**·3.2Me_2CO	**6**·4Me_2CO
Formula	$C_{88}H_{112}Cu_5Gd_2N_8O_{36}$	$C_{79.6}H_{95.2}Cu_5Dy_2N_8O_{33.2}$	$C_{80}H_{96}Cu_5Dy_2N_8O_{32}$
Fw	2490.05	2337.93	2324.34
Space group	$P\bar{1}$	$P\bar{1}$	$P2_1/c$
a (Å)	14.0383(3)	14.0857(9)	12.8953(3)
b (Å)	14.3830(3)	14.4462(8)	18.9026(4)
c (Å)	27.7492(6)	15.2281(10)	18.6798(5)
α (°)	95.011(1)	66.837(1)	90.0
β (°)	100.336(1)	70.385(2)	103.906(1)
γ (°)	112.363(1)	68.251(1)	90.0
V ($Å^3$)	5022.33(19)	2579.8(3)	4419.84(18)
Z	2	1	2
T (°C)	−113	293	−103
Radiation	Mo Kα 0.71073	Mo Kα 0.71073	Mo Kα 0.71073
ρ_{calcd} (g cm^{-3})	1.647	1.505	1.747
μ (mm^{-1})	2.426	2.516	2.936
Reflections with $I > 2\sigma(I)$	13 157	6768	7450
R_1[a]	0.0513	0.0703	0.0406
wR_2[a]	0.0963	0.1602	0.0722

$R_1 = \Sigma(|F_o|-|F_c|)/\Sigma(|F_o|)$ and $wR_2 = \{\Sigma[w(Fo^2-Fc^2)^2]/\Sigma[w(F_o^2)^2]\}^{1/2}$.
[a] $w = 1/[\sigma^2(F_o^2)+(\alpha P)^2 + bP]$ and $P = ((\max F_o^2,0) + 2F_c^2)/3$.

3420(br), ν(C=N) 1605(vs), ν_{as}(COO) 1508(s), ν_s(COO) 1342(s), ν(C–O) 1358(s), ν(C=O) 1700(m), $\nu(NO_3)_{coordinated}$ 1360(m)/1250 (m), $\nu(NO_3)_{ionic}$ 1380(vs).

2.2.3. $[Cu_5Dy_2(O_2CMe)_2(NO_3)_4(L1)_2(HL1)_2(Me_2CO)_2]3.2Me_2CO$ (3·3.2Me$_2$CO)

Solid $Dy(NO_3)_3{\cdot}6H_2O$ (0.10 mmol, 0.0439 g) was added under stirring to a yellow solution of H_3L1 (0.10 mmol, 0.0259 g) in Me_2CO (20 mL). After 10 min of stirring, solid $Cu(O_2CMe)_2{\cdot}H_2O$ (0.10 mmol,0.0200 g) was added and the solution became dark green. The stirring continued for 30 min and the final reaction solution was layered with mixture of Et_2O/*n*-hexane (1:1 v/v). Crystals of **3** were formed after five days. Yield: 0.0220 g, ~50% based on Cu^{II}. $C_{70}H_{76}N_8O_{30}Cu_5Dy_2$, **3** (f.w. = 2152.13) requires C, 39.07; H, 3.56; N, 5.21. Found: C, 38.98; H, 3.53; N, 5.17%. FT-IR (KBr pellets, selected peaks, cm^{-1}): ν(OH) 3420(br), ν(C=N) 1605(vs), ν_{as}(COO) 1510(s), ν_s(COO) 1340(s), ν(C–O) 1358(s), ν(C=O) 1701(m), $\nu\ (NO_3)_{coordinated}$ 1358(m)/1244(m), $\nu(NO_3)_{ionic}$ 1380(vs).

2.2.4. $[Cu_5Dy_2(O_2CMe)_2(NO_3)_4(L2)_2(HL2)_2]{\cdot}4Me_2CO$ (6·4Me$_2$CO)

Solid $Dy(NO_3)_3{\cdot}6H_2O$ (0.10 mmol, 0.0439 g) was added under stirring to a yellow solution of H_3L2 (0.10 mmol, 0.0273 g) in Me_2-CO (15 mL). After 10 min of stirring, solid $Cu(O_2CMe)_2{\cdot}H_2O$ (0.10 mmol, 0.0200 g) was added and the solution became dark green. The stirring continued for 30 min and the final reaction solution was layered with mixture of Et_2O/*n*-hexane (1:1 v/v). Crystals of **6**·4Me$_2$CO were formed after five days. Yield: 0.0099 g, ~20% based on Cu^{II}. $C_{80}H_{96}N_8O_{32}Cu_5Dy_2$, **6**·4Me$_2$CO (f.w. = 2324.21) requires C, 41.34; H, 4.16; N, 4.82. Found: C, 41.26; H, 4.13; N, 4.79%. FT-IR (KBr pellets, selected peaks, cm^{-1}): ν(OH) 3378(br), ν(C=N) 1605(vs), ν_{as}(COO) 1505(s), ν_s(COO) 1362(s), ν(C–O) 1355 (s), ν(C=O) 1700(m), $\nu(NO_3)_{coordinated}$ 1360(m)/1250(m), $\nu(NO_3)_{ionic}$ 1380(vs).

2.3. Single crystal X-ray crystallography

Crystals of **1**·6Me$_2$CO (0.15 × 0.20 × 0.30 mm) and **6**·4Me$_2$CO (0.06 × 0.08 × 0.20 mm), were taken from the mother liquor and immediately cooled to −113 (**1**) and −103 (**6**) °C, respectively. A crystal of **3**·3.2Me$_2$CO (0.15 × 0.30 × 0.30 mm) was mounted in capillary with drops of mother liquor. Diffraction measurements were made on a Rigaku R-AXIS SPIDER Image Plate diffractometer using graphite monochromated Mo Kα radiation. Data collection (ω-scans) and processing (cell refinement, data reduction and Empirical absorption correction) were performed using the CrystalClear program package [22]. The structures were solved by direct methods using shelxs-97 and refined by full-matrix least-squares techniques on F^2 with shelxl ver2014/6 [23]. Important crystallographic and refinement data are listed in Table 1. Further experimental crystallographic details for **1**·6Me$_2$CO: $2\theta_{max}$ = 52°; reflections collected/unique/used, 67984/19596 [R_{int} = 0.0698]/19596; 1384 parameters refined; $(\Delta/\sigma)_{max}$ = 0.000; $(\Delta\rho)_{max}/(\Delta\rho)_{min}$ = 0.991/−1.175 e/Å^3; *R*1/*wR*2 (for all data), 0.0891/0.1095. Further experimental crystallographic details for **3**·3.2Me$_2$CO: $2\theta_{max}$ = 52°; reflections collected/unique/used, 52815/10087 [R_{int} = 0.0710]/10087; 559 parameters refined; $(\Delta/\sigma)_{max}$ = 0.006; $(\Delta\rho)_{max}/(\Delta\rho)_{min}$ = 0.992/−1.627 e/Å^3; *R*1/*wR*2 (for all data), 0.1011/0.1807. Further experimental crystallographic details for **6**·4Me$_2$CO: $2\theta_{max}$ = 54°; reflections collected/unique/used, 53475/9607 [R_{int} = 0.0811]/9607; 661 parameters refined; $(\Delta/\sigma)_{max}$ = 0.000; $(\Delta\rho)_{max}/(\Delta\rho)_{min}$ = 0.993/−1.426 e/Å^3; *R*1/*wR*2 (for all data), 0.0599/0.0791. Hydrogen atoms were either located by difference maps and were refined isotropically or were introduced at calculated positions as riding on bonded atoms. All non-hydrogen atoms were refined anisotropically. Plots of the structures were drawn using the Diamond 3 program package [24].

3. Results and discussion

3.1. Synthesis and spectroscopic characterization

The reaction between $Ln(NO_3)_3{\cdot}6H_2O$ (Ln = Gd, Tb, Dy) and $Cu(O_2CMe)_2{\cdot}H_2O$ with the Schiff base ligands H_3L1 and H_3L2 in Me_2CO under stirring at room temperature afforded dark green solutions which gave green crystals (**1**, **2**, **3**, **6**) from closed vials and from layering of the reaction solution in mixture Et_2O/*n*-hexane (1:1 v/v), according to the following stoichiometric reactions:

$$2Ln(NO_3)_3\cdot 6H_2O + 5Cu(O_2CMe)_2\cdot H_2O + 4H_3L1 + 2Me_2CO \xrightarrow{Me_2CO} [Cu_5Ln_2(L1)_2(HL1)_2(NO_3)_4(O_2CMe)_2(Me_2CO)_2] + 2HNO_3 + 8MeCO_2H + 17H_2O \quad (1)$$

$$2Ln(NO_3)_3\cdot 6H_2O + 5Cu(O_2CMe)_2\cdot H_2O + 4H_3L2 \xrightarrow{Me_2CO} [Cu_5Ln_2(L2)_2(HL2)_2(NO_3)_4(O_2CMe)_2] + 2HNO_3 + 8MeCO_2H + 17H_2O \quad (2)$$

The above reactions were performed in different solvents (MeOH, MeCN etc) and also similar reactions involving other copper salts, e.g. chlorides, nitrates, perchlorates, gave microcrystalline or oily products which could not be further processed.

The IR spectra of **1**–**3** and **6** exhibit a broad band at ~3378 (**1**–**3**) and ~3420 (**6**) cm^{-1} attributed to the ν(OH) vibrations of the alkoxo groups of the protonated ligands. The bands at ~3060, ~2960 and ~2920 cm^{-1} are attributed to the ν(=CH), $\nu(CH_3)$ and $\nu(CH_2)$ stretching vibrations of the Schiff base and acetate ligands. A set of peaks in the 1600–1400 cm^{-1} region are attributed to the stretching vibrations of the α-substituted naphthalene ring and the strong band at ~745 cm^{-1} is attributed to the out-of-plane CH deformation vibrations of the naphthalene ring. The very strong band at ~1605 cm^{-1} is due to ν(C=N) vibration of the Schiff base ligands. This band appears at lower frequency with respect to the free ligands (1620 cm^{-1}) suggesting coordination of the metal ions through the imino nitrogen. The ν(C–O) stretching frequency of the phenolic oxygen of the free ligands is seen at 1396 cm^{-1} and shifts to ~1350–1360 cm^{-1} indicating coordination to the metal ions [25]. The medium intensity bands at ~1700 cm^{-1} are attributed to the ν(C=O) vibration of the coordinated and/or solvate Me_2CO molecules. The strong absorption bands at ~1250 and ~1360 cm^{-1} are attributed to the symmetric and antisymmetric vibrations of the coordinated nitrates [26]. The ν_{as}(C=O) and ν_s(C=O) are observed at ~1505 and ~1362 cm^{-1} (**1**–**3**) and 1510 and 1340 cm^{-1} (**6**) respectively. The difference Δ is ~143 cm^{-1} (**1**–**3**) and 170 cm^{-1} (**6**) as expected for the bridging mode of the acetate ligands. The strong band at ~1380 cm^{-1} is attributed to the presence of $\nu_3(E')$ [ν_d(NO)] mode of uncoordinated D_{3h} ionic nitrates; their presence is probably due to partial substitution of coordinated nitrates from bromides during the preparation of the KBr pellet under pressure [27].

3.2. Description of the structures

Complex **1** crystallizes in the triclinic space group *P*-1 and the asymmetric unit contains one cluster molecule and six acetone solvate molecules. Complex **3** also crystallizes in the triclinic space group *P*-1 and the asymmetric unit contains half of the complex and three acetone molecules with total occupancy 1.6. Complex **6** crystallizes in the monoclinic space group $P2_1/c$ and the asymmetric unit contains half of the complex and two acetone solvates. All complexes are neutral and consist of five Cu^{II} and two Ln^{III} ions which are held together via six μ_3-O_{alkoxo} and two μ_3-$O_{acetato}$ atoms. The topology of the central core, $\{Cu^{II}_5Ln^{III}_2(\mu_3\text{-}OR)_6(\mu_3\text{-}O_2CMe)_2\}^{8+}$, is described as two distorted cubane subunits,

$\{Cu^{II}_3Ln^{III}(\mu_3\text{-}OR)_3(\mu_3\text{-}O_2CMe)\}^{5+}$, with a common apex on Cu(1). All three complexes present similar metal topology and coordination (Fig. S1a, b), therefore only the crystal structure of **1** will be described in detail. Complex **6** is isomorphous to complexes **4** and **5** described previously [7]. The molecular structures of complexes **1**, **3** and **6** are shown in Figs. 1–3, respectively. Selected bond distances are listed in Tables 2–4.

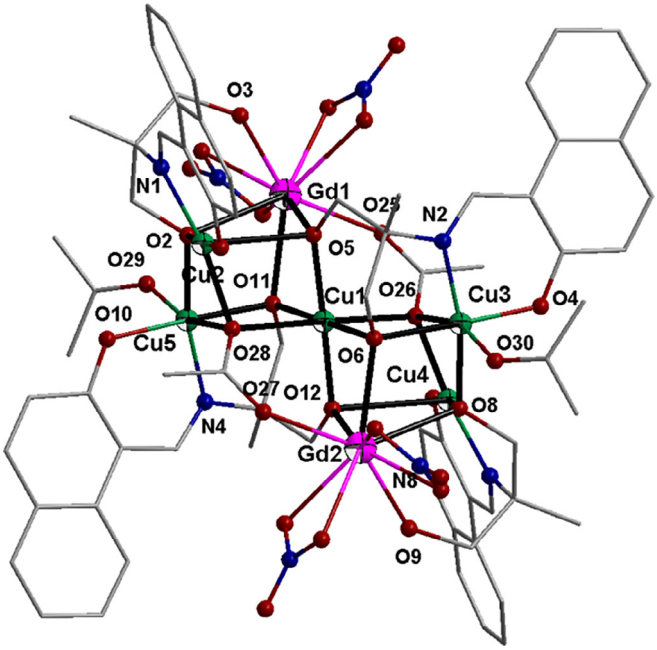

Fig. 1. Partially labeled plot of **1**. The metal core is highlighted in black. Color code: Gd magenta, Cu green, O red, N blue, C light grey. (Colour online.)

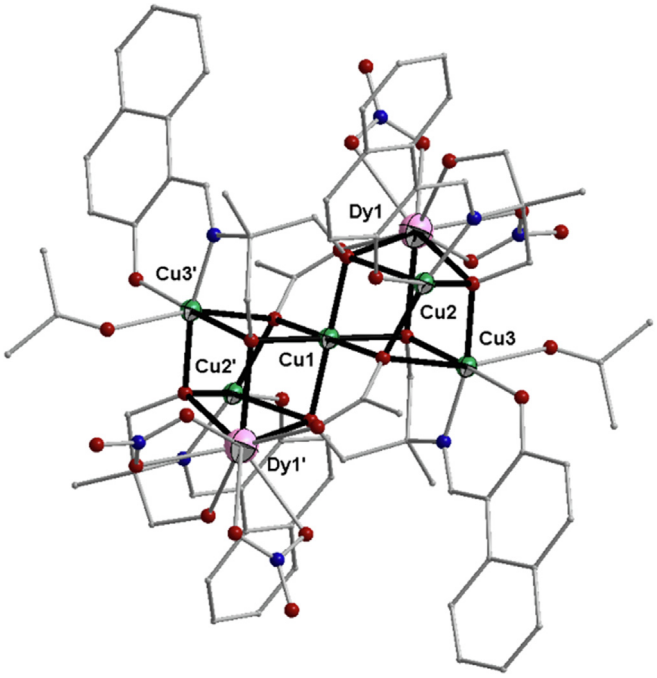

Fig. 2. Partially labeled plot of **3**. The metal core is highlighted in black. Color code: Dy pink, Cu green, O red, N blue, C light grey. Primed atoms are generated by symmetry: (′) $1-x, -y, -z$. (Colour online.)

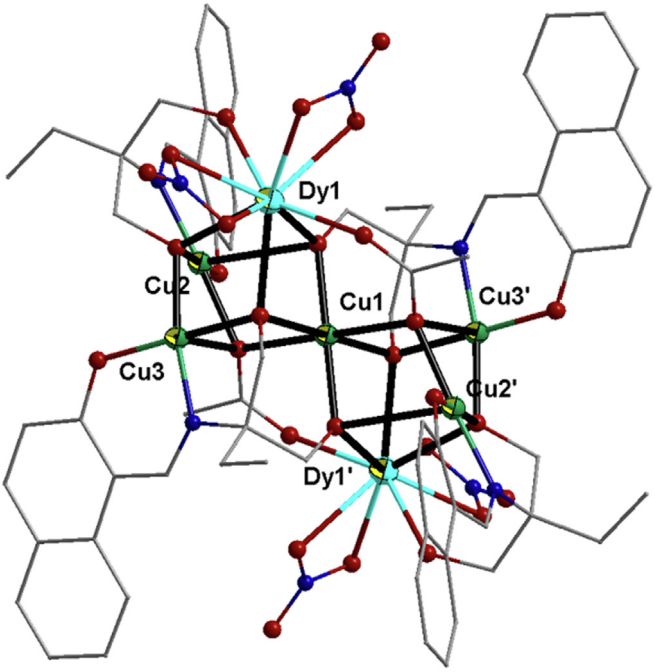

Fig. 3. Partially labeled plot of **6**. The metal core is highlighted in black. Color code: Dy cyan, Cu green, O red, N blue, C light grey. Primed atoms are generated by symmetry: (′) $-x, 1-y, 2-z$. (Colour online.)

Table 2
Selected bond distances (Å) in **1**·6Me_2CO.

Gd1–O5	2.304 (4)	Gd2–O12	2.292 (4)
Gd1–O25	2.395 (4)	Gd2–O27	2.397 (4)
Gd1–O3	2.409 (4)	Gd2–O6	2.418 (4)
Gd1–O11	2.416 (4)	Gd2–O9	2.441 (4)
Gd1–O17	2.470 (4)	Gd2–O23	2.481 (4)
Gd1–O14	2.491 (4)	Gd2–O19	2.485 (4)
Gd1–O16	2.492 (4)	Gd2–O20	2.491 (4)
Gd1–O13	2.494 (4)	Gd2–O22	2.507 (4)
Gd1–O2	2.594 (4)	Gd2–O8	2.596 (4)
Cu1–O5	1.963 (4)	Cu3–O4	1.894 (4)
Cu1–O12	1.974 (4)	Cu3–N2	1.897 (5)
Cu1–O6	1.996 (4)	Cu3–O8	1.953 (4)
Cu1–O11	2.003 (4)	Cu3–O6	1.989 (3)
Cu1–O28	2.392 (4)	Cu3–O26	2.589 (5)
Cu1–O26	2.394 (4)	Cu3–O30	2.481 (6)
Cu2–O1	1.889 (4)	Cu4–O7	1.887 (4)
Cu2–N1	1.915 (5)	Cu4–N3	1.909 (5)
Cu2–O2	1.990 (4)	Cu4–O26	1.985 (4)
Cu2–O28	1.992 (4)	Cu4–O8	1.986 (4)
Cu2–O5	2.657 (4)	Cu4–O12	2.764 (4)
Cu5–O10	1.902 (4)	Cu5–O11	1.993 (4)
Cu5–N4	1.905 (5)	Cu5–O28	2.561 (5)
Cu5–O2	1.960 (4)	Cu5–O29	2.515 (6)

Table 3
Selected bond distances (Å) in **3**·3.2Me_2CO.

Dy1–O6′	2.265 (4)	Cu1–O14′	2.412 (5)
Dy1–O13	2.366 (6)	Cu1–O14	2.412 (5)
Dy1–O3	2.396 (6)	Cu2–O1	1.879 (5)
Dy1–O5	2.397 (5)	Cu2–N1	1.928 (7)
Dy1–O7	2.451 (6)	Cu2–O2	1.984 (5)
Dy1–O11	2.461 (6)	Cu2–O14′	1.990 (6)
Dy1–O10	2.472 (5)	Cu2–O6	2.756 (6)
Dy1–O8	2.473 (6)	Cu3–N2	1.897 (7)
Dy1–O2	2.597 (5)	Cu3–O4	1.903 (5)
Cu1–O6	1.958 (5)	Cu3–O2	1.963 (6)
Cu1–O6′	1.958 (5)	Cu3–O5	1.991 (5)
Cu1–O5	2.010 (4)	Cu3–O14	2.568 (6)
Cu1–O5′	2.010 (4)	Cu3–O15	2.552 (6)

Symmetry operation: (′) $1-x, -y, -z$.

Table 4
Selected bond distances (Å) in **6**·4Me_2CO.

Dy1–O13′	2.247 (3)	Cu1–O41	2.456 (2)
Dy1–O42	2.362 (3)	Cu1–O41′	2.456 (2)
Dy1–O12	2.398 (3)	Cu2–O1	1.884 (3)
Dy1–O3	2.403 (3)	Cu2–N1	1.916 (3)
Dy1–O22	2.432 (3)	Cu2–O41′	1.986 (3)
Dy1–O32	2.441 (3)	Cu2–O2	2.013 (3)
Dy1–O21	2.456 (3)	Cu2–O13′	2.886 (2)
Dy1–O31	2.490 (3)	Cu3–O11	1.882 (3)
Dy1–O2	2.557 (3)	Cu3–N11	1.902 (3)
Cu1–O13	1.959 (3)	Cu3–O2	1.955 (3)
Cu1–O13′	1.959 (3)	Cu3–O12	1.975 (3)
Cu1–O12	1.993 (3)	Cu3–O41′	2.492 (3)
Cu1–O12′	1.993 (3)		

Symmetry operation: (′) $-x$, $1-y$, $2-z$.

The seven metal ions in **1** are held together via two $L1^{3-}$ and two $HL1^{2-}$ ligands and two μ_3-κ^3O: $\kappa O'$ $MeCO_2^-$ ligands. The triply deprotonated ligands, $L1^{3-}$, behave as μ_5-κ^3O, κ^3O', $\kappa O''$, κN (Scheme 1) and bridge the central Cu(1) with a Cu/Gd pair belonging to each of the cubane subunits, thus bridge three Cu^{II} and two Gd^{III} ions. The $L1^{3-}$ ligand defined by atoms O(4)/N(2)/O(5)/O(6) chelates around Cu(3) through the $O_{phenoxo}$ (O(4)), N_{imino} (N(2)) and O_{alkoxo} (O(6)) atoms; the latter is also coordinated to Gd(2) and Cu(1), thus acting as μ_3-bridge. The second deprotonated O_{alkoxo} (O(5)) of $L1^{3-}$ ligand coordinates to Cu(1) and also to Cu (2) and Gd(1), acting also as μ_3-bridge. The second $L1^{3-}$ ligand defined by atoms O(10)/N(4)/O(11)/O(12) chelates around Cu(5) through the $O_{phenoxo}$ (O(10)), N_{imino} (N(4)) and O_{alkoxo} (O(11)) atoms; the latter is also coordinated to Gd(1) and Cu(1), thus acting as μ_3-bridge. The second deprotonated O_{alkoxo} (O(12)) of $L1^{3-}$ ligand coordinates to Cu(1) and also to Cu(4) and Gd(2), acting also as μ_3-bridge. The doubly deprotonated ligands, $HL1^{2-}$, behave as μ_3-κ^3O, $\kappa O'$, $\kappa O''$, κN (Scheme 1) and bridge two Cu^{II} and one Gd^{III} of each cubane subunit. The $HL1^{2-}$ ligand defined by O(1)/N(1)/O (2)/O(3) chelates around Cu(2) through the $O_{phenoxo}$ (O(1)), N_{imino} (N(1)) and O_{alkoxo} (O(2)) atoms; the latter is also coordinated to Gd(1) and Cu(5), thus acting as μ_3-bridge. The protonated O_{alkoxo}, O(3), is coordinated to Gd(1). The second deprotonated $HL1^{2-}$ ligand defined by O(7)/N(3)/O(8)/O(9) chelates around Cu(4) through the $O_{phenoxo}$ (O(7)), N_{imino} (N(3)) and O_{alkoxo} (O(8)) atoms; the latter is also coordinated to Gd(2) and Cu(3), thus acting as μ_3-bridge. The protonated O_{alkoxo}, O(9), is coordinated to Gd(2).

Cu(1) presents distorted octahedral coordination geometry consisting of two deprotonated O_{alkoxo} atoms from two L^{3-} ligands (O (5)/O(6) and O(12)/O(13)) with Cu(1)–O_{alkoxo} in the range 1.963 (4)–2.003(4) Å in the equatorial plane, and two μ_3-acetato oxygen atoms (O(26)/O(28)) in the apical positions with Cu(1)–$O_{acetato}$ ~2.39 Å. Cu(2) and Cu(4) are five-coordinate with square pyramidal geometry. The equatorial plane in Cu(2) is defined by atoms O(1)/N(1)/O(2) of one $HL1^{2-}$ and O(28) of one μ_3-$O_{acetate}$ with bond distances in the range 1.889(4)–1.992(4) Å and the apical position is occupied by O(5) of one $L1^{3-}$ at 2.657(4) Å. The equatorial plane in Cu(4) is defined by atoms O(7)/N(3)/O(8) of one $HL1^{2-}$ and O(26) of one μ_3-$O_{acetate}$ with bond distances in the range 1.887(4)–1.986 (4) Å and the apical position is occupied by O(12) of one $L1^{3-}$ at 2.764(4) Å. The trigonality index τ is 0.1 and 0.04 for Cu(2) and Cu(4), respectively. Cu(3) and Cu(5) are six-coordinate with distorted octahedral geometry. Cu(3) coordinates to O(4)/N(2)/O(6) of one $L1^{3-}$ and O(8) of one $HL1^{2-}$ with bond distances in the range 1.894(4)-1.953(4) Å in the equatorial plane, whereas the apical positions are occupied by O(26) of one μ_3-$O_{acetate}$ and O(30) of one monodentate Me_2CO with bond distances 2.589(5) and 2.481 (6) Å, respectively. Cu(5) coordinates to O(10)/N(4)/O(11) of one $L1^{3-}$ and O(2) of one $HL1^{2-}$ with bond distances in the range 1.902(4)–1.993(4) Å in the equatorial plane, whereas the apical positions are occupied by O(28) of one μ_3-$O_{acetate}$ and O(29) of one monodentate Me_2CO with bond distances 2.561(5) and 2.515 (6) Å, respectively.

The coordination sphere around each Gd^{III} ion consists of nine oxygen atoms, two μ_3-O_{alkoxo} from two $L1^{3-}$, one μ_3-O_{alkoxo} and one protonated μ_3-O_{alkoxo} from one $HL1^{2-}$, the monodentate $O_{acetato}$ atom, and four oxygen atoms from two chelate NO_3^- ions. The bond distances around Gd(1) and Gd(2) are in the range 2.304(4)–2.594(4) and 2.292(4)–2.596(4) Å, respectively. Continuous Shape Measures by using the program SHAPE [28] show that the best-fit polyhedron around the Ln^{III} ions in **1**, **3** and **6** is the spherical capped antiprism CSAPR-9 (CShM = 1.10597/1.25291, 1.15555 and 1.21208 for **1**, **3** and **6**, respectively). All metal ions in **6** present the same ligation as in **1** and **3**, however the lack of the two coordinated Me_2CO molecules, result in square pyramidal geometry for the peripheral Cu^{II} ions, Cu(3)/Cu(3′) (Fig. S1c–e).

The protonated alkoxo group of each $HL1^{2-}$ in **1** participates in hydrogen bond with one of the Me_2CO solvate molecules [O(3)···O (31) = 2.743 Å, HO(3)···O(31) = 2.152 Å, O(3)–HO(3)···O(31) = 145.4°; O(9)···O(32) = 2.734 Å (1 + x, y, z), HO(9)···O(32) = 1.964 Å, O(9)–HO(9)···O(32) = 156.0°]. The same type of hydrogen bond is observed in **3** [O(3)···O(16′) (1 − x, −y, −z) = 2.764 Å, HO(3)···O(16′) = 2.024 Å, O(3)–HO(3)···O(16′) = 146.8°] and in **6** [O(3)···O(51′) (−x, 0.5 + y, 1.5-z) = 2.678 Å, HO(3)···O(51′) = 1.983 Å, O(3)–HO(3)···O(51′) = 159.1°].

3.3. Magnetic measurements

Magnetic susceptibility measurements as a function of temperature were recorded from polycrystalline samples of **1**–**3** and **6** at 1000 Oe dc field. The $\chi_M T$ product for **1** at 300 K is 15.26 cm^3 - $Kmol^{-1}$. This value is lower than the theoretical value of 17.625 cm^3 $Kmol^{-1}$ for five Cu^{II} ions (S = 1/2 with C = 0.375 cm^3 - $Kmol^{-1}$, g = 2) and two Gd^{III} ions (S = 7/2 with C = 7.875 cm^3 - $Kmol^{-1}$, g = 2). The $\chi_M T$ product increases gradually upon cooling reaching the value of 18.11 cm^3 $Kmol^{-1}$ at 20 K and then it increases rapidly to the value of 23.13 cm^3 $Kmol^{-1}$ at 2 K (Fig. 4). The overall temperature dependence of the $\chi_M T$ product suggests the presence of dominant ferromagnetic interactions between the five Cu^{II} and the two Gd^{III} ions. The magnetization measurements at 2.5 K as a function of the external applied field show a rapid increase upon increasing of the magnetic field reaching a value of 16.52 N μ_B at 8 T (Fig. 4). This value is lower than the value of 19 μ_B expected for two Gd^{III} (S = 7/2) ions and five Cu^{II} (S = 1/2) ions which are uncoupled or completely ferromagnetically coupled (S_T = 19/2), suggesting that some of the metal ions are antiferromagnetically coupled. This can be tentatively attributed to the opposite spin arrangement of the central Cu^{II} with respect to the other metal ions, thus leading to a total ground spin state of S = 17/2 (spin-up vs spin-down model). The saturation value of

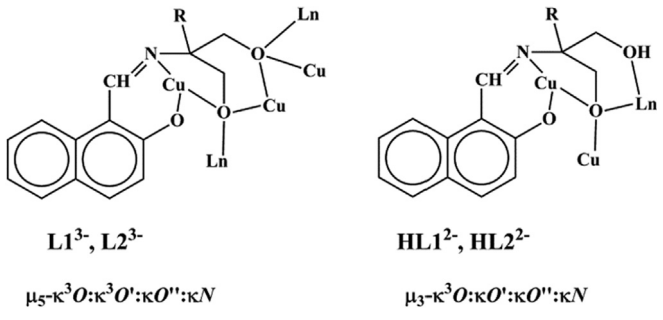

Scheme 1. The coordination modes of $L1^{3-}$/$L2^{3-}$ and $HL1^{2-}$/$HL2^{2-}$ ligands in **1**, **3** and **6**.

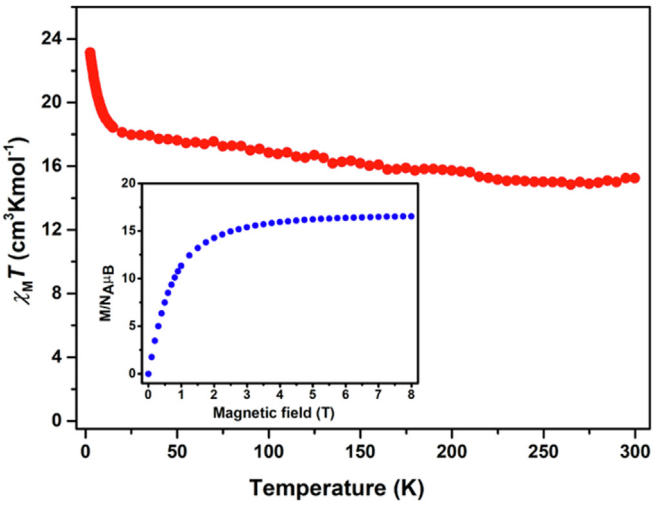

Fig. 4. $\chi_M T$ vs T plots for **1** at 1000 Oe and magnetization curve at 2.5 K (inset).

the magnetization should be then equal to 17 μ_B which is close to the experimental value of 16.52 μ_B. The clear saturation above 4 T suggests the presence of an isolated ground state of low magnetic anisotropy. The magnetic behavior of **1** is analogous to the behavior of complex **4** which we reported earlier [7].

Isothermal magnetization plots in the 2–12 K temperature range under external applied magnetic field up to 5 T for **1** are shown in Fig. 5a. These data can be used to evaluate the magnetocaloric effect (MCE) of **1** by calculating the magnetic entropy changes $-\Delta S_m$ according to Maxwell equation

$$-\Delta S_m(T)_{\Delta H} = \int [\vartheta M(T,H)/\vartheta T]_H dH \quad (3)$$

or by using the simpler numerical approximation to the above integral [29]

$$|\Delta S_m| = \sum_i \frac{M_i - M_{1+1}}{T_i - T_{1+1}} \Delta H_i \quad (4)$$

where M_i and M_{i+1} are the experimental values of magnetization at T_i and T_{i+1} temperatures, respectively, under an applied field of intensity H_i. The experimental values of the magnetic entropy change obtained from the experimental isothermal magnetization curves under various magnetic field variations are shown in Fig. 5b. The maximum entropy change of 16.3 J kg^{-1} K^{-1} is obtained at 2 K for ΔH = 5 T. This value is lower than the theoretically calculated value for **1**, according to equation

$$-\Delta S_m = \frac{R}{2.2578}\sum_i \ln(2S_i+1) = \frac{R}{2.2578}\left[5\ln\left(2\frac{1}{2}+1\right)+2\ln\left(2\frac{7}{2}+1\right)\right] = 28.1\ \text{Jkg}^{-1}\text{K}^{-1} \quad (5)$$

considering that the two Gd^{III} (S = 7/2) and the five Cu^{II} (S = 1/2) ions in **1** are fully decoupled. The maximum entropy change obtained in several Cu-Gd complexes of various nuclearities and metal topologies fall in the range 11.9–34.5 J kg^{-1} K^{-1} for 2.0–4.5 K and ΔH = 7 T [30–34].

The $\chi_M T$ product for **2** at 300 K is 25.82 cm^3 Kmol^{-1} which is slightly larger than the theoretical value of 25.50 cm^3 Kmol^{-1} for five Cu^{II} ions (S = 1/2 with C = 0.375 cm^3 Kmol^{-1}, g = 2) and two Tb^{III} ions (S = 3, L = 3, J = 6 with C = 11.81 cm^3 Kmol^{-1}, g = 3/2). The $\chi_M T$ product increases gradually upon lowering the temperature and reaches the value of 61.85 cm^3 Kmol^{-1} at 5.25 K and then drops to 45.38 cm^3 Kmol^{-1} at 2 K (Fig. 6). The overall temperature dependence of the $\chi_M T$ product suggests the presence of dominant ferromagnetic interactions between the five Cu^{II} and the two Tb^{III} ions. The large value of $\chi_M T$ product at 2 K suggests the presence of a large spin ground state. The magnetization measurements at 2 K as a function of the external applied field show a rapid increase upon increasing of the magnetic field reaching a value of 19.47 N μ_B at 8 T (Fig. 6); this value is lower than the value of 23 μ_B expected for two Tb^{III} (J = 6, g = 3/2) ions and five Cu^{II} (S = 1/2, g = 2) ions which are uncoupled or completely ferromagnetically coupled. This behavior indicates the presence of magnetic anisotropy and/or possibly low-lying excited states. The overall magnetic behavior of **2** is analogous to that of the congener complex **5** which we reported earlier [7].

The dynamic magnetic properties of **2** were investigated by ac magnetic susceptibility measurements as a function of temperature at different frequencies under external field of 1000 Oe. The

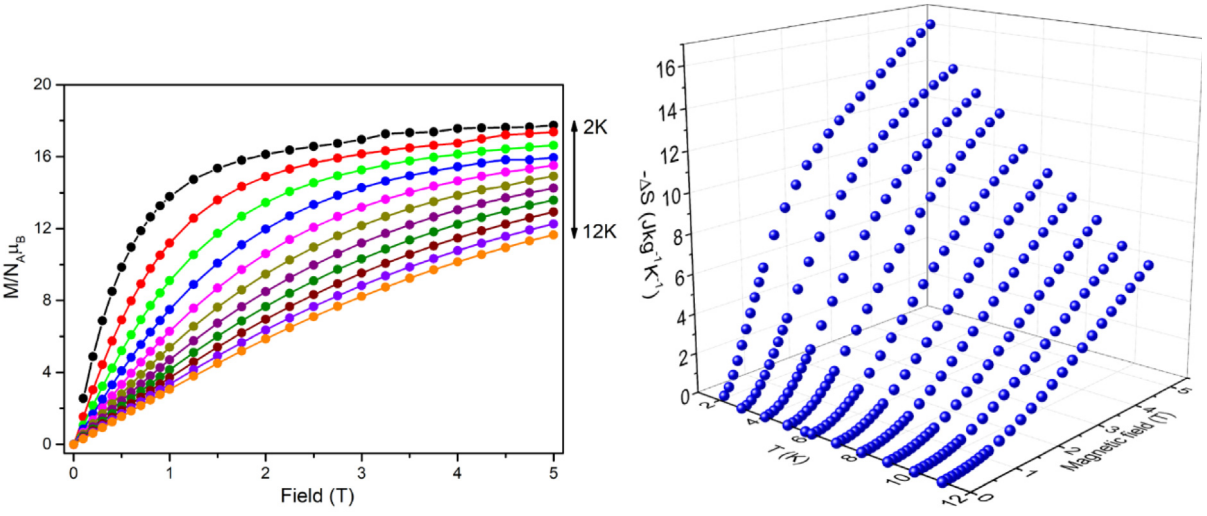

(a) **(b)**

Fig. 5. (a) Field-dependent magnetization plots for **1** at 2–12 K. (b) 3D plots of experimental $-\Delta S_m$ values in 2–12 K and 0–5 T for **1**.

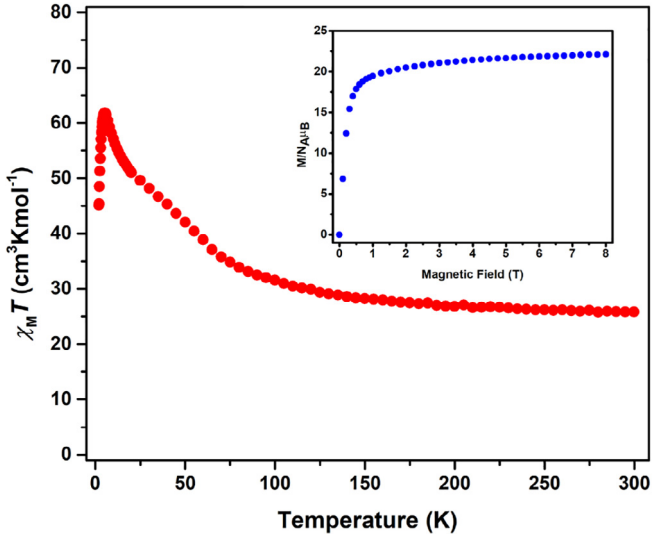

Fig. 6. $\chi_M T$ vs T plots for **2** at 1000 Oe and magnetization curve at 2 K (inset).

plots of in-phase and out-of-phase ac magnetic susceptibilities at low temperatures under 1000 Oe dc field are shown in Fig. S2a. The data show that the out-of-phase magnetic susceptibility deviates very slightly from zero at temperatures below 3 K and is frequency dependent. No maximum in χ'' is observed down to 2 K, which is the lowest temperature for our setup. The ac susceptibility data can be approximated with the Debye model with $\ln(\chi''/\chi') = \ln(\omega\tau_0) + U_{eff}/k_BT$ ($\omega = 2\pi\nu$) [35], considering that the relaxation of the magnetization occurs through a single process, and hence, the energy barrier U_{eff}/k_B and τ_0 values can be estimated. The linear fit to the $\ln(\chi''/\chi')$ vs 1/T data gave $U_{eff}/k_B = 1.3 \pm 0.1$ K and pre-exponential factor $\tau_0 = 3.0 \pm 0.2 \times 10^{-6}$ s for **2** (Fig. S2b).

The $\chi_M T$ product for **3** at 300 K is 38.69 cm^3 Kmol^{-1} which is larger than the theoretical value of 30.21 cm^3 Kmol^{-1} for five Cu^{II} ions ($S = 1/2$ with $C = 0.375$ cm^3 Kmol^{-1}, $g = 2$) and two Dy^{III} ions ($S = 5/2$, $L = 5$, $J = 15/2$ with $C = 14.17$ cm^3 Kmol^{-1}, $g = 4/3$). The $\chi_M T$ product increases gradually upon decreasing the temperature and reaches the value of 98.28 cm^3 Kmol^{-1} at 2.75 K and then takes the value of 95.31 cm^3 Kmol^{-1} at 2 K (Fig. 7). The overall temperature dependence of the $\chi_M T$ product suggests the presence of dominant ferromagnetic interactions between the five Cu^{II} and the two Dy^{III} ions and a large spin ground state. The magnetization

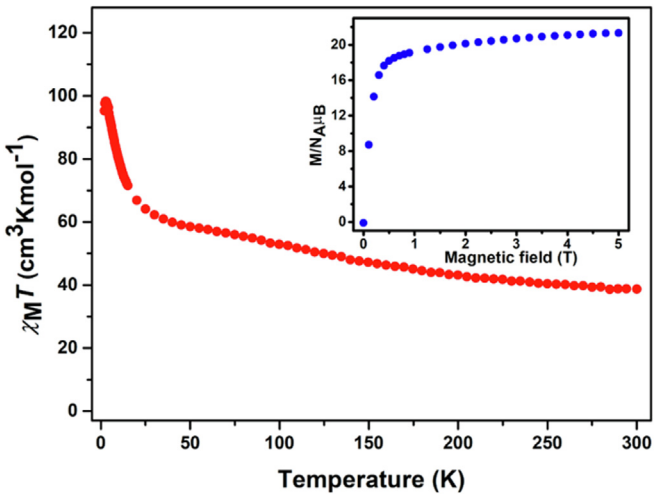

Fig. 7. $\chi_M T$ vs T plots for **3** at 1000 Oe and magnetization curve at 2 K (inset).

measurements at 2 K as a function of the external applied field show a rapid increase upon increasing of the magnetic field reaching a value of 21.33 N μ_B at 5 T (Fig. 7) without reaching saturation; this value is lower than the value of 25 μ_B expected for two Dy^{III} ($J = 15/2$, $g = 4/3$) ions and five Cu^{II} ($S = 1/2$, $g = 2$) ions which are uncoupled or completely ferromagnetically coupled.

The dynamic magnetic properties of **3** were investigated by ac susceptibility measurements in the temperature range 2–15 K under zero applied magnetic field and at frequencies in the range 50–10000 Hz. Out-of-phase peaks are clearly seen in the χ'' vs T plots above 2.5 K and at frequencies above 1000 Hz (Fig. 8) suggesting that **3** behaves as single-molecule magnet (SMM) under these experimental conditions.

The plot of χ'' vs χ' (Cole-Cole plot) for **3** in the temperature range 2.2–4.2 K at zero dc field is shown in Fig. 9. A first attempt to simulate these data with the Debye model (one relaxation time) represented by a semicircle with radius $(1/2 - \chi_s/2\chi_T)$ and center the point $(1/2 + \chi_s/2\chi_T, 0)$ do not reproduce appropriately the experimental data. The data can be reproduced using the Cole-Cole model [36]. In this model the relaxation time follows a distribution,

$$f(\tau) = \frac{1}{2\pi} \times \frac{\sin(\alpha\pi)}{\cosh[(1-\alpha)\ln(\tau/\tau_0)] - \cos\alpha\pi}$$

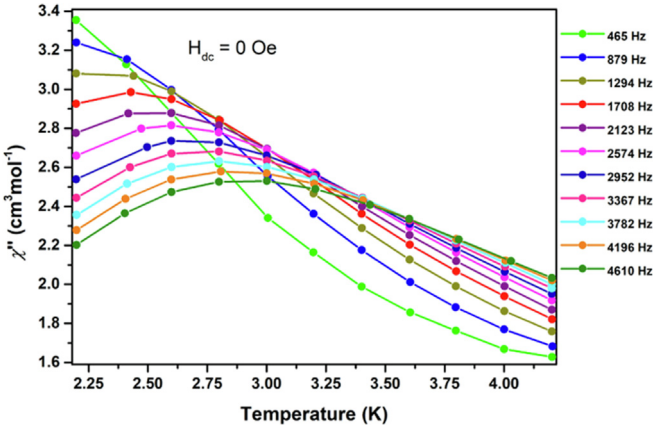

Fig. 8. Temperature dependence of χ'' of **3** at different frequencies under zero applied external field.

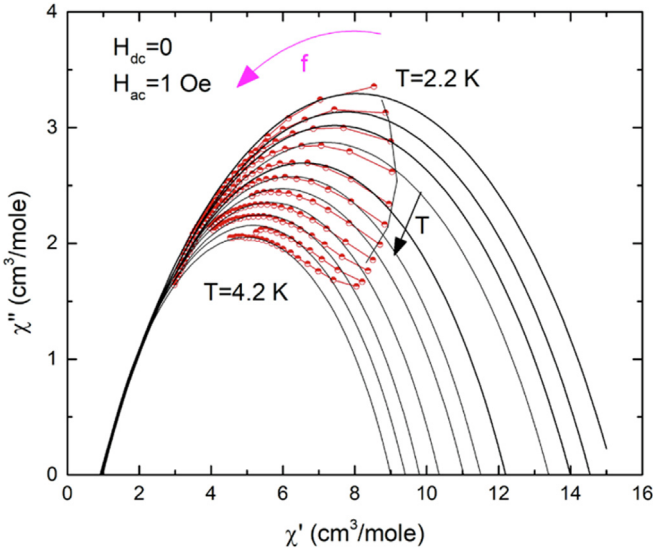

Fig. 9. χ'' vs χ' plots for **3** at zero external field. The solid lines represent the simulation semicircles according to equation (7).

resulting in a complex ac magnetic susceptibility given by the equation

$$\chi = \chi_S + \frac{(\chi_T - \chi_S)}{1 + (i\omega\tau)^{1-\alpha}} \quad (6)$$

where χ_T is the isothermal susceptibility i.e. the susceptibility in zero frequency, and χ_S is the adiabatic susceptibility i.e. the susceptibility at high frequencies. α is an empirical constant related to the effective width of the relaxation time distribution. The magnetic susceptibility equation is equivalent to the circle equation with its center sifted to negative values

$$\left(\chi' - \frac{\chi_T + \chi_S}{2}\right)^2 + \left(\chi'' + \frac{\chi_T - \chi_S}{2}\cot[(1-\alpha)\pi/2\right)^2 = \left(\frac{\chi_T - \chi_S}{2}\mathrm{cosec}[(1-\alpha)\pi/2\right)^2 \quad (7)$$

The curves shown in Fig. 9 are reproduced using an $\alpha = 0.4$–0.5. The temperature variation of the parameters α, χ_T and χ_S are shown in supplementary material (Fig. S3a). Using the frequency which corresponds to maximum value of the semicircles the relaxation time, was estimated ($\tau = 1/2\pi f$). By means of Arrhenius plot, the energy barrier ($U_{eff}/k_B = 13(5)$ K) and the pre-exponential factor, ($\tau_0 = 1.2(5) \times 10^{-6}$ s) were estimated (Fig. S3b).

The $\chi_M T$ product for **6** at 300 K is 27.67 cm^3 $Kmol^{-1}$ which is smaller than the theoretical value of 30.21 cm^3 $Kmol^{-1}$ for five Cu^{II} ions ($S = 1/2$ with $C = 0.375$ cm^3 $Kmol^{-1}$, $g = 2$) and two Dy^{III} ions ($S = 5/2$, $L = 5$, $J = 15/2$ with $C = 14.17$ cm^3 $Kmol^{-1}$, $g = 4/3$). The $\chi_M T$ product increases gradually upon decreasing the temperature and reaches the value of 51.92 cm^3 $Kmol^{-1}$ at 15 K and then takes the value of 13.00 cm^3 $Kmol^{-1}$ at 2 K (Fig. 10). The overall temperature dependence of the $\chi_M T$ product suggests the presence of dominant ferromagnetic interactions between the five Cu^{II} and the two Dy^{III} ions and a large spin ground state. The magnetization measurements at 3 K as a function of the external applied field show a rapid increase upon increasing of the magnetic field reaching a value of 17.77 N μ_B at 8 T (Fig. 10) without reaching saturation; this value is lower than the value of 25 μ_B expected for two Dy^{III} ($J = 15/2$, $g = 4/3$) ions and five Cu^{II} ($S = 1/2$, $g = 2$) ions which are uncoupled or completely ferromagnetically coupled.

The dynamic magnetic properties of **6** were investigated by ac magnetic susceptibility measurements as a function of temperature (2–6 K) at different frequencies under zero external field. The plots of in-phase and out-of-phase ac magnetic susceptibilities at low temperatures under zero dc field shown in Fig. 11. The data show that the out-of-phase magnetic susceptibility deviates from zero at temperatures below 4 K and is frequency dependent. No maximum in χ'' is observed down to 2 K, which is the lowest temperature for our setup. Application of an external dc field of 1000 Oe did not affect the ac signal profile (Fig. S4).

The plot of χ'' vs χ' (Cole-Cole plot) for **6** in the temperature range 2–4 K at zero dc field are shown in Fig. 12.

Similarly with the case of **3,** the ac magnetic susceptibility spectra can be reproduced by the Cole-Cole model [36]. Moreover, despite the complicate topology of the magnetic ions, this simple model with a distribution of relaxation times, capture the essential features of the ac susceptibility spectra. The curves shown in Fig. 12 have been calculated using values for α from 0.5 (lower temperature) to 0.445 (T = 4 K). The temperature variation of α, χ_T and χ_S, used to calculate these curves, are shown in the supplementary material (Fig. S5a). Using the frequency which corresponds to maximum value of the semicircles, the relaxation time, was estimated ($\tau = 1/2\pi f$). By means of Arrhenius plot, the energy barrier ($U_{eff}/k_B = 9.9(4)$ K) and the pre-exponential factor, ($\tau_0 = 1.2(2)\text{x}10^{-6}$ s) were estimated (Fig. S5b).

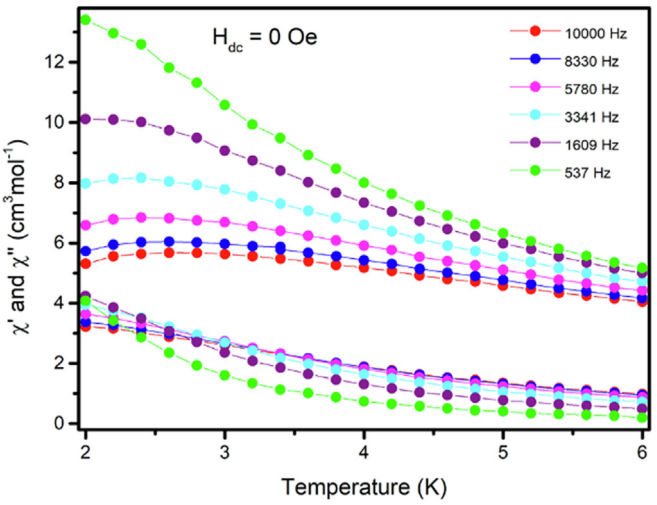

Fig. 11. Temperature dependence of χ' and χ'' of **6** under different frequencies under zero external field.

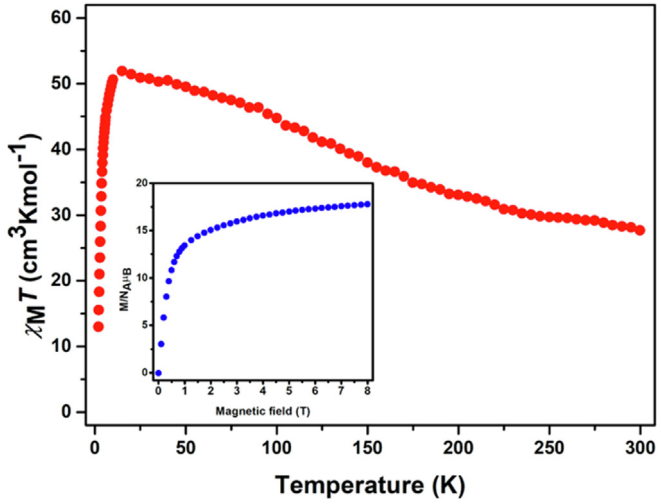

Fig. 10. (a) $\chi_M T$ vs T plots for **6** at 1000 Oe and magnetization curve at 3 K (inset).

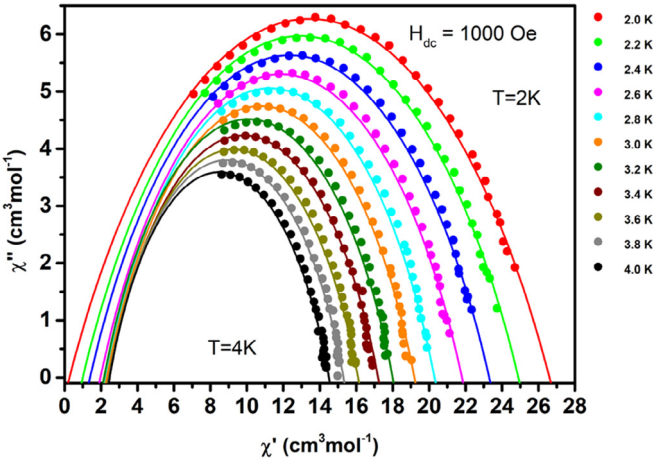

Fig. 12. χ'' vs χ' plots for **6** at zero external field. The solid lines represent the simulation semicircles according to Eq. (7).

4. Conclusions

The use of the polydentate Schiff base ligands, H_3L1 and H_3L2 ($OH\text{-}C_{10}H_6\text{-}CH{=}NC(R)(CH_2OH)_2$, R = CH_3, H_3L1; R = C_2H_5, H_3L2) with $Cu(O_2CMe)_2{\cdot}H_2O$ and $Ln(NO_3)_3{\cdot}6H_2O$ (Ln = Gd, Tb, Dy) in Me_2CO solutions gave new members of the family of heterometallic heptanuclear complexes with the general formula $[Cu_5Ln_2(O_2CMe)_2(NO_3)_4(L1)_2(HL1)_2(Me_2CO)_2]$ (Ln = Gd (**1**), Tb (**2**), Dy (**3**)) and $[Cu_5Ln_2(O_2CMe)_2(NO_3)_4(L2)_2(HL2)_2]$ (Ln = Gd (**4**), Tb (**5**), Dy (**6**)); complexes **4** and **5** were reported previously by us [7]. All six complexes consist of five Cu^{II} and two Ln^{III} ions held together through two $L1^{3-}$ or $L2^{3-}$ and two $HL1^{2-}$ or $HL2^{2-}$ ligands, two $\mu_3\text{-}\kappa^3O$: κ O′ $MeCO_2^-$ ligands and four chelating nitrates. The metal topology is described as two distorted $\{Cu_3Ln\}$ cubane subunits with a common apex on a Cu^{II} ion. The magnetic susceptibility measurements for all six complexes indicate dominant ferromagnetic interactions between the metal ions. Complexes **1** and **4** display a ground state of spin $S = 17/2$, as indicated by magnetization measurements. This can be explained considering that the central Cu^{II} ion is antiferromagnetically coupled to the Cu_4Gd_2 moiety. Isothermal magnetization studies for **1** and **4** yielded maximum entropy change of 16.3 J kg^{-1} K^{-1} at 2 K under $\Delta H = 5$ T for **1** and 15.7 J kg^{-1} K^{-1} at 2 K under $\Delta H = 5$ T for **4**. Ac magnetic susceptibility measurements for complexes **2**, **5** and **6** show the presence of tails in the out-of-phase vs T plots at various frequencies in the temperature range 2–6 K under zero external field. The values of the out-of-phase ac susceptibility are frequency dependent. Application of an external field of 1000 Oe did not alter the ac signal profiles. These tails are characteristic of the presence of slow relaxation of the magnetization below 2 K which is the lowest limit of our setup. Ac susceptibility measurements for **3** show clear maxima in the out-of-phase vs T plots above 2.5 K and at frequencies above 1000 Hz. These peaks are characteristic of slow relaxation of the magnetization and single-molecule behavior for complex **3**. The Cole-Cole plots for **3** and **6** revealed that the data cannot be reproduced by the Debye model through one relaxation process, and that the relaxation time follows a distribution according to the Cole-Cole model with values α in the range 0.4–0.5 (for **3**) and 0.445–0.5 (for **6**). The Arrhenius plots yielded $U_{eff}/k_B = 13(5)$ K and $\tau_0 = 1.2(5) \times 10^{-6}$ s for **3**, and $U_{eff}/k_B = 9.9(4)$ K and $\tau_0 = 1.2(2)$ $x10^{-6}$ s for **6**. More work is in progress to enrich this family of heptanuclear $\{Cu^{II}_5Ln^{III}_2\}$ complexes with other members containing different lanthanide ions and of course the diamagnetic Y^{III} and/or La^{III} analogues in order to prepare multifunctional complexes whose properties would be governed by the nature of the lanthanide ion and the type of the magnetic exchange between the metal ions.

Acknowledgements

This research is implemented through IKY Scholarships Programme and co-financed by the European Union (European Social Fund – ESF) and Greek national funds through the action entitled "Reinforcement of Postdoctoral Researchers", in the framework of the Operational Programme "Human Resources Development Programme, Education and Lifelong Learning" of the National Strategic Reference Framework (NSRF) 2014–2020.

Appendix A. Supplementary data

CCDC 1908959, 1908960 and 1908961 contains the supplementary crystallographic data for **1**, **3** and **6**. These data can be obtained free of charge via http://www.ccdc.cam.ac.uk/conts/retrieving.html, or from the Cambridge Crystallographic Data Centre, 12 Union Road, Cambridge CB2 1EZ, UK; fax: (+44) 1223-336-033; or e-mail: deposit@ccdc.cam.ac.uk. Figures of structure overlay and metal coordination for **1**, **3** and **6**; χ''/χ' vs T and $\ln(\chi''/\chi')$ vs $1/T$ for **2** under 1000 Oe dc field; temperature variation of parameters α, χ_T and χ_S, τ vs $1/T$ plots for **3** and **6**; χ''/χ' vs T plots for **6** under 1000 Oe. Supplementary data to this article can be found online at https://doi.org/10.1016/j.poly.2019.05.004.

References

[1] G. Christou, Polyhedron 24 (2005) 2065.
[2] Molecular Nanomagnets and Related Phenomena, Ed. S. Gao, Struct. Bond. 164 (2015).
[3] G. Lorusso, J.W. Sharples, E. Palacios, O. Roubeau, E.K. Brechin, R. Sessoli, A. Rossin, F. Tuna, E.J.L. McInnes, D. Collison, M. Evangelisti, Adv. Mater. 25 (2013) 4653.
[4] J.-L. Liu, Y.-C. Chen, F.-S. Guo, M.-L. Tong, Coord. Chem. Rev. 281 (2014) 26.
[5] S. Zhang, P. Cheng, Chem. Rec. 16 (2016) 2077.
[6] Single-Molecule Magnets, Molecular Architectures and Building Blocks for Spintronics, Ed. M. Holyńska, Wiley-VCH Verlag GmbH & Co., 2019, pp. 23–25.
[7] D. Dermitzaki, O. Bistola, M. Pissas, V. Psycharis, Y. Sanakis, C.P. Raptopoulou, Polyhedron 150 (2018) 47.
[8] R. Koner, H.-H. Lin, H.-H. Wei, S. Mohanta, Inorg. Chem. 44 (2005) 3524.
[9] J.-P. Costes, B. Donnadieu, R. Gheorghe, G. Novitchi, J.-P. Tuchagues, L. Vendier, Eur. J. Inorg. Chem. (2008) 5235.
[10] M. Towatari, K. Nishi, T. Fujinami, N. Matsumoto, Y. Sunatsuki, M. Kojima, N. Mochida, T. Ishida, N. Re, J. Mrozinski, Inorg. Chem. 52 (2013) 6160.
[11] R. Gheorghe, M. Andruh, J.-P. Costes, B. Donnadieu, M. Schmidtmann, A. Müller, Inorg. Chim. Acta 360 (2007) 4044.
[12] L. Xu, Q. Zhang, G. Hou, P. Chen, G. Li, D.M. Pajerowski, C.L. Dennis, Polyhedron 52 (2013) 91.
[13] J.-P. Costes, S. Shova, W. Wernsdorfer, Dalton Trans. 37 (2008) 1843.
[14] J.-P. Costes, M. Auchel, F. Dahan, V. Peyrou, S. Shova, W. Wernsdorfer, Inorg. Chem. 45 (2006) 1924.
[15] T. Hamamatsu, K. Yabe, M. Towatari, S. Osa, N. Matsumoto, N. Re, A. Pochaba, J. Mrozinski, J.-L. Gallani, A. Barla, P. Imperia, C. Paulsen, J.-P. Kappler, Inorg. Chem. 46 (2007) 4458.
[16] S. Osa, T. Kido, N. Matsumoto, N. Re, A. Pochaba, J. Mrozinski, J. Am. Chem. Soc. 126 (2004) 420.
[17] V. Chandrasekhar, A. Dey, S. Das, M. Rouzières, R. Clérac, Inorg. Chem. 52 (2013) 2588.
[18] L. Jiang, B. Liu, H.-W. Zhao, J.-L. Tian, X. Liu, S.-P. Yan, CrystEngComm 17 (2017) 1816.
[19] A. Dey, S. Das, S. Kundu, A. Mondal, M. Rouzières, C. Mathonière, R. Clérac, R. Suriya Narayanan, V. Chandrasekhar, Inorg. Chem. 56 (2017) 14612.
[20] G. Wu, I.J. Hewitt, S. Mameri, Y. Lan, R. Clérac, C.E. Anson, S. Qiu, A.K. Powell, Inorg. Chem. 46 (2007) 7229.
[21] C.P. Raptopoulou, Y. Sanakis, V. Psycharis, M. Pissas, Polyhedron 64 (2013) 181.
[22] M.S.C. Rigaku, CrystalClear, Rigaku/MSC Inc., The Woodlands, Texas, USA, 2005.
[23] (a) G.M. Sheldrick, Acta Crystallogr., Part A 64 (2008) 112;
(b) G.M. Sheldrick, Acta Crystallogr., Part C 71 (2015) 3.
[24] DIAMOND – Crystal and Molecular Structure Visualization, Ver. 3.1, Crystal Impact, Rathausgasse 30, 53111, Bonn, Germany.
[25] K. Mounika, B. Anupama, J. Pragathi, C. Gyanakumari, J. Sci. Res. 2 (2010) 513.
[26] L.J. Bellamy, The Infra-red Spectra of Complex Molecules, Chapman and Hall, London, 1975.
[27] K. Nakamoto, Infrared and Raman Spectra of Inorganic and Coordination Compounds, fourth ed., Wiley, New York, 1986.
[28] M. Llunell, D. Casanova, J. Girera, P. Alemany, S. Alvarez, SHAPE, version 2.0, Barcelona, Spain, 2010.
[29] F. Torres, X. Bohigas, J.M. Hernández, J. Tejada, J. Phys.: Condens. Matter 15 (2003) L119.
[30] (a) S.K. Langley, N.F. Chilton, B. Moubaraki, T. Hooper, E.K. Brechin, M. Evangelisti, K.S. Murray, Chem. Sci. 2 (2011) 1166;
(b) T.N. Hooper, J. Schnack, S. Piligkos, M. Evangelisti, E.K. Brechin, Angew. Chem., Int. Ed. 51 (2012) 4633.
[31] (a) J.-D. Leng, J.-L. Liu, M.-L. Tong, Chem. Commun. 48 (2012) 5286;
(b) J.-L. Liu, Y.-C. Chen, Q.-W. Li, S. Gomez-Coca, D. Aravena, E. Ruiz, W.-Q. Lin, J.-D. Leng, M.-L. Tong, Chem. Commun. 49 (2013) 6549;
(c) J.-L. Liu, W.-Q. Lin, Y.-C. Chen, S. Gómez-Coca, D. Aravena, E. Ruiz, J.-D. Leng, M.-L. Tong, Chem. Eur. J. 19 (2013) 17567.
[32] (a) H. Zhang, G.-L. Zhuang, X.-J. Kong, Y.-P. Ren, L.-S. Long, R.-B. Huang, L.-S. Zheng, Cryst. Growth Des. 13 (2013) 2493;
(b) D. Dermitzaki, G. Lorusso, C.P. Raptopoulou, V. Psycharis, A. Escuer, M. Evangelisti, S.P. Perlepes, T.C. Stamatatos, Inorg. Chem. 52 (2013) 10235;
(c) P. Richardson, D.I. Alexandropoulos, L. Cunha-Silva, G. Lorusso, M. Evangelisti, J. Tang, T.C. Stamatatos, Inorg. Chem. Front. 2 (2015) 945.
[33] (a) T.N. Hooper, R. Inglis, M.A. Palacios, G.S. Nichol, M.B. Pitak, S.J. Coles, G. Lorusso, M. Evangelisti, E.K. Brechin, Chem. Commun. 50 (2014) 3498;
(b) S. Xue, Y.-N. Guo, L. Zhao, H. Zhang, J. Tang, Inorg. Chem. 53 (2014) 8165.
[34] T. Rajeshkumar, H.V. Annadat, M. Evangelisti, S.K. Langley, N.F. Chilton, K.S. Murray, G. Rajaraman, Inorg. Chem. 54 (2015) 1661.
[35] J. Bartolome, G. Filoti, V. Kuncser, G. Schinteie, V. Mereacre, C.E. Anson, A.K. Powell, D. Prodius, C. Turta, Phys. Rev. B 80 (2009) 014430.
[36] K.S. Cole, R.H. Cole, J. Chem. Phys. 9 (1941) 341.